EJN fens European Journal of Neuroscience

European Journal of Neuroscience, Vol. 30, pp. 1306–1317, 2009 doi:10.1111/j.1460-9568.2009.06922.x

NEUROSYSTEMS

Frequency-selectivity of a thalamocortical relay neuron during Parkinson's disease and deep brain stimulation: a computational study

Hayriye Cagnan,[1] Hil G. E. Meijer,[2] Stephan A. van Gils,[2] Martin Krupa,[5] Tjitske Heida,[2] Michelle Rudolph,[3] Wytse J. Wadman[4] and Hubert C. F. Martens[1]

[1]Philips Research Laboratories, High Tech Campus, Eindhoven 5656 AE, Netherlands
[2]University of Twente, Enschede, Netherlands
[3]CNRS, Integrative and Computational Neuroscience Unit 1, Gif-Sur-Yvette, France
[4]SILS-Center for Neuroscience, University of Amsterdam, Amsterdam, Netherlands
[5]Radboud University, Nijmegen, Netherlands

Keywords: basal ganglia, high-frequency stimulation, modulation, relay

Abstract

In this computational study, we investigated (i) the functional importance of correlated basal ganglia (BG) activity associated with Parkinson's disease (PD) motor symptoms by analysing the effects of globus pallidus internum (GPi) bursting frequency and synchrony on a thalamocortical (TC) relay neuron, which received GABAergic projections from this nucleus; (ii) the effects of subthalamic nucleus (STN) deep brain stimulation (DBS) on the response of the TC relay neuron to synchronized GPi oscillations; and (iii) the functional basis of the inverse relationship that has been reported between DBS frequency and stimulus amplitude, required to alleviate PD motor symptoms [A. L. Benabid *et al.* (1991) *Lancet*, **337**, 403–406]. The TC relay neuron selectively responded to and relayed synchronized GPi inputs bursting at a frequency located in the range 2–25 Hz. Input selectivity of the TC relay neuron is dictated by low-threshold calcium current dynamics and passive membrane properties of the neuron. STN-DBS prevented the TC relay neuron from relaying synchronized GPi oscillations to cortex. Our model indicates that DBS alters BG output and input selectivity of the TC relay neuron, providing an explanation for the clinically observed inverse relationship between DBS frequency and stimulus amplitude.

Introduction

Deep brain stimulation (DBS) is a treatment for late-stage Parkinson's disease (PD) during which high-frequency electrical stimuli are chronically delivered to targets such as subthalamic nucleus (STN), globus pallidus internum (GPi) or ventral intermediate nucleus of the thalamus (Th). Clinically effective stimulation parameters (stimulus frequency 120–180 Hz, stimulus amplitude 1–5 V, pulse width 60–200 μs) have been determined empirically and are accepted as benchmark values (Benabid, 2003). Benabid *et al.* (1991) observed an inverse relationship between stimulation frequency and amplitude, indicating that for lower stimulation frequencies, suppression of PD motor symptoms can only be achieved with increased stimulus amplitude (Gao *et al.*, 1999; Rizzone *et al.*, 2001; Moro *et al.*, 2002).

PD motor symptoms (e.g. bradykinesia, rigidity and tremor) are directly correlated with enhanced synchronized activity of the basal ganglia (BG) in the theta (3–10 Hz) and beta (15–30 Hz) bands (Levy *et al.*, 2000, 2002; Brown & Williams, 2005; Chen *et al.*, 2007). It has also been noted that suppression of PD motor symptoms due to treatment (e.g. L-dopa, DBS) is linked to suppression of synchronized BG activity in these frequencies (Brown *et al.*, 2001, 2004; 2005). Based on these observations, Brown (2003) hypothesized that thalamus relays anti-kinetic BG oscillation frequencies to cortex (CTX), giving rise to PD motor symptoms, and that DBS results in alleviation of the motor symptoms by suppressing enhanced activity in the theta and beta bands in the thalamo-cortico-basal ganglia loop.

Despite the high clinical efficacy of DBS, a consensus regarding the underlying mechanism of action is lacking (Dostrovsky & Lozano, 2002). Experimental studies have indicated that DBS results in somatic block and subsequent elimination of enhanced synchronized activity in the BG, giving rise to alleviation of PD motor symptoms (Beurrier *et al.*, 2001; Tai *et al.*, 2003). Nevertheless, modelling studies have suggested that myelinated axons, within the activation field of the electrode, can exhibit synchronous activity at the DBS frequency, despite block of neuronal activity at the soma (Holsheimer, 2002; McIntyre *et al.*, 2004). Activation of axons during DBS could potentially spread the high-frequency activity to other nuclei, under

Correspondence: H. Cagnan, as above.
E-mail: hayriye.cagnan@philips.com

Received 22 July 2008, revised 10 July 2009, accepted 30 July 2009

the assumption that synaptic depression and/or depolarization block do not occur (Lozano *et al.*, 2002; Hashimoto *et al.*, 2003; Brown *et al.*, 2004; Miocinovic *et al.*, 2006). Building on these observations, Rubin & Terman (2004) have demonstrated that thalamocortical (TC) relay capability is restored, due to low-threshold calcium current dynamics, when the oscillatory BG input to the neuron is fully overwritten by high-frequency input (Rubin & Terman, 2004). However, their study did not specifically address for which conditions BG oscillations are relayed by TC relay neurons to CTX and the mechanism behind the frequency–amplitude dependency of DBS. To address these issues, we investigate TC relay neuron frequency selectivity during PD and STN-DBS and, based on cellular dynamics, provide an explanation for the inverse relationship between DBS frequency and stimulus amplitude.

Materials and methods

We investigated frequency-selective properties of TC relay neurons during PD using two TC relay neuron models, a morphologically realistic multi-compartment model and a single-compartment model (Table 1 and Appendix). We also studied the changes that occur in frequency-selective properties of TC relay neurons during STN-DBS by incorporating a BG network model (Rubin & Terman, 2004) projecting onto the single-compartment TC relay neuron model (Fig. 1).

TABLE 1. Parameters for the soma and the dendritic tree of the TC relay neuron

Parameter	Value
E_{Na}	45 mV
E_K	−95 mV
E_h	−43 mV
g_{Na}	0.03 S/cm^2
g_K	0.003 S/cm^2
g_{Ks}	0.0007 S/cm^2
g_h	0.0005 S/cm^2
g_{Naleak}	0.000015 S/cm^2
g_{Kleak}	0.00005 S/cm^2

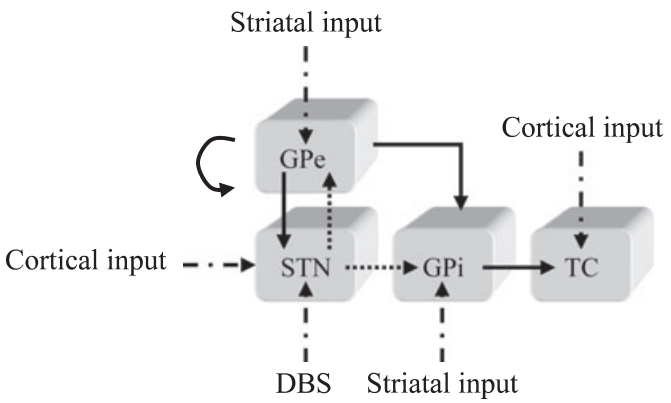

FIG. 1. Nuclei and connections incorporated in the network model, which is used in the simulations investigating the effects of STN-DBS on the TC relay neuron functionality. Solid lines indicate inhibitory synaptic connections between nuclei while dashed lines indicate excitatory synaptic connections between nuclei. External input (e.g. DBS, projection from striatum to GPe, striatum to GPi, projection from CTX to STN or projection from CTX to thalamus) is indicated by dash-dot lines.

Section A: TC frequency selectivity during PD

Multi-compartment and single-compartment TC relay neuron model

The multi-compartment TC relay neuron model, consisting of 208 compartments (Huguenard & Prince, 1992; Destexhe *et al.*, 1998), was downloaded from ModelDB (http://senselab.med.yale.edu/modeldb/) and simulated in the NEURON environment (Hines & Carnevale, 1997). The membrane current equation for compartment i connected to k branches that relate the voltage V_i to the membrane currents I_{ion} is:

$$C_m(dV_i/dt) = -(I_{Na,i} + I_{K,i} + I_{T,i} + I_{h,i} + I_{Ks,i} + I_{Naleak,i} + I_{Kleak,i} + I_{GPi-Th,i} - (V_{i-1} - V_i)g_{i-1,i} - \sum_k (V_{i+k} - V_i)g_{i,i+k}) \quad (1)$$

Detailed analysis was performed on a simplified single-compartment model representing the soma of the TC relay neuron which was implemented in MATLAB (Mathworks, Inc., Natick, MA, USA). Membrane potential (V_m) of the single-compartment model is described by:

$$C_m\left(\frac{dV_m}{dt}\right) = -(I_{Na} + I_K + I_T + I_h + I_{Ks} + I_{Naleak} + I_{Kleak} + I_{GPi-Th} + I_{CTX-Th} + I_{app}) \quad (2)$$

Ion current descriptions and maximum ion channel conductance used in the single-compartment model and the multi-compartmental model can be found in the Appendix and Table 1.

GPi projection in the multi-compartment model

Neuronal tracings indicate that a group of GPi neurons converge on a single TC relay neuron (Smith *et al.*, 1998). We modelled the effect of the GABAergic GPi projection by implementing conductance-based exponential synapses (Equations 1 and 3). At compartment i, synaptic density (ρ) was equivalent to 0.025 synapses/μm^2 (Smith *et al.*, 1998). The total number of synapses at a given compartment was set to the floor of $A_i\rho$, i.e. rounded down to the nearest integer ($\lfloor A_i\rho \rfloor$), where A_i is the area of compartment i:

$$I_{GPi-Th,i}(t) = 1/A_i\left(\sum_j g_{GABA,j}(t)(V_i - E_{GABA})\right) \; 0 \le j \le \lfloor A_i\rho \rfloor \quad (3)$$

$g_{GABA,j}$ is the conductance of synapse j and E_{GABA} is the synaptic reversal potential (−85 mV) (Kim *et al.*, 1997; Terman *et al.*, 2002; McIntyre *et al.*, 2004; Rubin & Terman, 2004).

At synapse j, an artificially generated spike train, modelling the firing pattern of a single pre-synaptic GPi neuron, was received. This artificially generated spike train contained bursts of 50 ms duration, which consisted of eight spikes on average (Raz *et al.*, 2000; Wichmann *et al.*, 2002). The time interval between bursts modelled the bursting frequency (f_{GPi}) of a GPi neuron and the variation between burst arrival times ($\delta t = N(0,\sigma)t_{start}$) at different synapses was used as a measure of the level of correlation (C) between pre-synaptic GPi neurons (Raz *et al.*, 2000). When the correlation was $0 \le C \le 1$, spike arrival times were normally distributed with mean 0 and variance (σ) of $(1–C)/C$. When a spike was observed at synapse j, $g_{GABA,j}$ was instantaneously incremented by 0.5 nS and decayed exponentially with a time constant of 10 ms (Rudolph & Destexhe, 2006).

GPi projection in the single-compartment model

In order to reflect the essential properties of the multi-compartment synaptic input (see Supporting information, Fig. S1), the GABAergic GPi projection was modelled as an oscillatory signal with phase noise:

$$I_{\mathrm{GPI-Th}}(t) = g_{\mathrm{GPi-Th}}(1 + \alpha \sin(\varphi(t)))(V_{\mathrm{m}} - E_{\mathrm{GABA}}) \quad (4)$$

where E_{GABA} is the synaptic reversal potential (−85 mV) (Kim *et al.*, 1997; Terman *et al.*, 2002; McIntyre *et al.*, 2004; Rubin & Terman, 2004), $g_{\mathrm{GPi\text{-}Th}}$ is the mean synaptic conductance, α is the modulation depth (between 0 and 1) and $\varphi(t)$ is the phase of the oscillatory conductance change. The temporal evolution of the phase $\varphi(t)$ of the oscillatory input is modelled by:

$$\varphi(t + dt) = \varphi(t) + 2\pi f_{\mathrm{GPi}} dt + N(0, \sigma)\sqrt{dt} \quad (5)$$

where f_{GPi} defines the average bursting frequency of the GPi input and $N(0,\sigma)$ defines the phase noise as a random number drawn from a normal distribution with mean 0 and variance σ.

Cortical projection in the single-compartment model

In addition to the GABAergic GPi input, TC relay neurons receive excitatory projections from the pre-motor and supplementary motor CTX. Connections between TC relay neurons and CTX are predominantly reciprocal but can also contain non-reciprocal components (McFarland & Haber, 2002). The relaying capability of the TC relay neuron in the physiological state, PD and STN-DBS was tested with excitatory, conductance-based, synaptic current $I_{\mathrm{CTX\text{-}Th}}$ modelling cortical input (Rubin & Terman, 2004; Guo *et al.*, 2008; Pirini *et al.*, 2009):

$$I_{\mathrm{CTX-Th}} = g_{\mathrm{CTX-Th}} H(\sin(2\pi t f_{\mathrm{CTX}})) (1 - H(\sin(2\pi(t + \delta_{\mathrm{CTX}}) f_{\mathrm{CTX}})))(V_{\mathrm{m}} - E_{\mathrm{Glut}}) \quad (6)$$

where $g_{\mathrm{CTX\text{-}Th}}$ is the mean synaptic conductance, f_{CTX} is the frequency and δ_{CTX} is the duration of the cortical input. The reversal potential for the cortical synaptic input (E_{Glut}) is set at 0 mV. H refers to the Heaviside step function, where $H(x)$ is zero for $x < 0$ and is equivalent to 1 when $x > 0$.

Section B: TC frequency selectivity during DBS

Network model

The BG network model used to investigate frequency-selective properties of the TC relay neuron during STN-DBS is an extension of the network model described in Rubin & Terman (2004). STN, globus pallidus externum (GPe) and GPi neurons are modelled using single-compartment conductance-based equations (Terman *et al.*, 2002; Rubin & Terman, 2004; Pirini *et al.*, 2009). We have replaced the TC relay neuron model described in Rubin & Terman (2004) with the single-compartment TC relay neuron described in Section A and the Appendix. The network model includes 16 STN, 16 GPe, 16 GPi neurons and one TC relay neuron. Each STN neuron receives inhibitory input from two GPe neurons and each GPe neuron receives excitatory input from three STN neurons and inhibitory input from two GPe neurons. Each GPi neuron receives excitatory input from three STN neurons and inhibitory input from two GPe neurons. All GPi neurons project onto the same TC relay neuron. Parameters defining the properties of STN, GPe and GPi neurons and properties of the network are the same as those described in Rubin & Terman (2004) and Pirini *et al.* (2009), unless explicitly mentioned in the Appendix. The network has only been simulated in the parkinsonian state (Rubin & Terman, 2004; Pirini *et al.*, 2009).

The model includes the following external inputs: (i) striatum to GPe (indirect pathway), (ii) striatum to GPi (direct pathway), (iii) CTX to STN (hyper-direct pathway) and (iv) CTX to TC relay neuron (Rubin & Terman, 2004; Pirini *et al.*, 2009). Recent experimental studies indicate that the hyper-direct pathway plays a crucial role in the generation of sustained oscillations in the BG nuclei in the beta frequency bands during PD (Baufreton *et al.*, 2005; Wilson *et al.*, 2006; Hammond *et al.*, 2007). Therefore, we included the hyper-direct pathway from CTX to STN represented as:

$$I_{\mathrm{CTX-STN}} = g_{\mathrm{CTX-STN}}(1 + \sin(2\pi f_{\mathrm{CTX-STN}} t))(V_{\mathrm{m}} - E_{\mathrm{Glut}}) \quad (7)$$

where $f_{\mathrm{CTX\text{-}STN}}$ is the frequency of the cortical input and is set at 15 Hz (Levy *et al.*, 2000). $g_{\mathrm{CTX\text{-}STN}}$ is the mean synaptic conductance and is equivalent to 1 pA/μm^2.

Deep brain stimulation

The effect of DBS on STN neurons is modelled as a train of pulses injected into STN neurons (Rubin & Terman, 2004):

$$I_{\mathrm{DBS}} = i_{\mathrm{D}} H(\sin(2\pi f_{\mathrm{DBS}} t))(1 - H(\sin(2\pi f_{\mathrm{DBS}}(t + \delta)))) \quad (8)$$

where i_D is the amplitude of the current injection and is set at 400 pA/μm^2, δ is the duration of a single pulse and is set to 3 ms, and f_{DBS} represents the frequency of the pulse train and is equivalent to the frequency of DBS. As in Equation 6, H represents the Heaviside step function. Based on the notion that DBS activation volume is dependent on stimulus amplitude (Butson & McIntyre, 2005; Butson *et al.*, 2007), we assume a monotonic relationship between stimulus voltage and percentage of neurons activated due to DBS. The percentage of STN neurons activated due to DBS is represented by varying the number of STN neurons receiving I_{DBS}. Somatic block due to DBS is not modelled in this study as activated STN neurons receive both I_{DBS} and $I_{\mathrm{CTX\text{-}STN}}$.

Quantification of TC relay functionality

Several studies have linked BG activity patterns in the theta and beta frequency bands to PD motor symptoms (Levy *et al.*, 2000, 2002; Hutchison *et al.*, 2004; Fogelson *et al.*, 2005; Chen *et al.*, 2006, 2007; Trottenberg *et al.*, 2007) and suppression of these activities with alleviation of PD motor symptoms (Brown *et al.*, 2001, 2004; 2005; Hammond *et al.*, 2007).

Building on the notion that pathophysiology and treatment efficacy relate to frequency content in the thalamo-cortico-basal ganglia loop, we used spectral analysis (fast Fourier transform) to quantify functionality of a TC relay neuron which received excitatory cortical, inhibitory GPi and under certain conditions DBS-induced inputs. TC relay functionality was evaluated by comparing the frequency content of binary spike trains obtained from the TC output to the frequency contents of the various input signals. The influence of DBS-induced activity on TC relay functionality was assessed by the level of suppression of GPi burst frequencies in the TC output (Brown *et al.*, 2004; Hammond *et al.*, 2007). The level of suppression of GPi burst frequencies was quantified by measuring the change in the magnitude of GPi burst frequencies during DBS with respect to the magnitude of GPi burst frequencies during PD.

Results

Section A: TC frequency selectivity during PD

Response to GABAergic GPi projection in the multi-compartment TC relay neuron model

First, the response of a TC relay neuron to inhibitory GPi projection was studied. The response of the multi-compartment TC relay neuron

was investigated as a function of pre-synaptic correlation (C) while bursting frequency (f_{GPi}) of the pre-synaptic GPi neurons was kept constant. When the pre-synaptic correlation was above a critical value, the neuron fired action potentials due to the inhibitory input from the GPi at the bursting frequency of the pre-synaptic GPi neurons (Fig. 2B). For pre-synaptic correlations below the critical correlation level, the membrane potential at the soma exhibited sub-threshold oscillations at the bursting frequency of the pre-synaptic GPi neurons (Fig. 2A). The previous analysis was repeated for various frequencies in order to understand how the response to correlation level changes for different pre-synaptic bursting frequencies. We observed that the TC relay neuron exhibited frequency-dependent selectivity to pre-synaptic correlation levels for firing action potentials and as the bursting frequency of the GPi neurons varied, the critical correlation level above which the TC relay neuron fired action potentials shifted. The same analysis was performed for non-bursting GPi inputs and showed similar results (data not shown). Figure 2C shows the selectivity curve of a TC relay neuron. It defines the boundary between sub-threshold oscillation (Fig. 2A) and action potential generation (Fig. 2B) in response to inhibitory GPi projection at the GPi bursting frequency. Figure 2C also shows that there exists an optimum frequency (i.e. GPi bursting frequency) at which a minimum amount of pre-synaptic correlation is required to drive the TC relay neuron at the GPi bursting frequency.

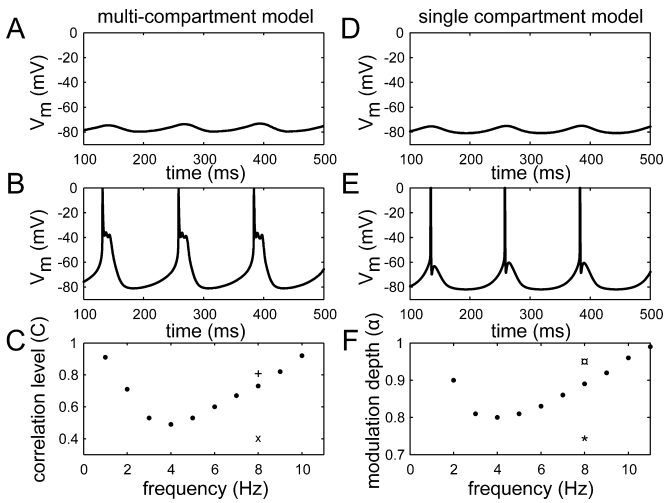

FIG. 2. Selective TC response to correlated, bursting GPi inputs. Results obtained using the multi-compartment model and the single-compartment model are shown in A–C and D–F, respectively. (A) The membrane potential oscillates between the resting membrane potential and a relatively hyperpolarized value when GPi burst frequency is equivalent to 8 Hz and the correlation level (C) among the GPi neurons is 0.4 (f_{GPi} and C values are indicated with an 'x' in C). (B) TC relay neuron fires action potentials at the GPi burst frequency (8 Hz) when the correlation level (C) among the GPi neurons is 0.8 (f_{GPi} and C values are indicated with a '+' in C). (C) Selectivity curve defining the boundary between GPi burst frequencies and correlation levels which induce action potential generation at GPi burst frequency (parameters above the selectivity curve) and GPi burst frequencies and correlation levels that lead to sub-threshold oscillation of the TC relay neuron's membrane potential (parameters below the selectivity curve) (resting membrane potential = −65 mV). (D) The membrane potential oscillates between the resting membrane potential and a relatively hyperpolarized value when the GPi burst frequency is 8 Hz and input modulation depth (α) is 0.75 (f_{GPi} and α values are indicated with an '*' in F). (E) TC relay neuron fires action potentials at the GPi burst frequency (8 Hz) when the modulation depth (α) is 0.95 (f_{GPi} and α values are indicated with an '¤' in F). (F) Selectivity curve when the resting membrane potential is −65 mV describing GPi burst frequency and modulation depth selectivity of the single-compartment TC relay neuron (for D–F $g_{GPi\text{-}Th}$ = 0.2 mS/cm^2).

Response to GABAergic GPi projection in the single-compartment TC relay neuron model

The analysis in the multi-compartment model was repeated in the single-compartment TC relay neuron model in order to test whether the response to inhibitory GPi projection was preserved and realistically represented in the reduced model with simplified synaptic input. When the GPi burst frequency was at 8 Hz and modulation depth of the reduced synaptic input was set at 0.75, the membrane potential in the single-compartment TC relay neuron model showed sub-threshold oscillations (Fig. 2D). When the synaptic input was set at a higher modulation depth (0.95) at the same GPi burst frequency, the model responded with action potentials (Fig. 2E). Figure 2F shows the selectivity curve of a TC relay neuron obtained using the single-compartment model. The selectivity curves of the single- and multi-compartment model are qualitatively equivalent (Fig. 2C and F), given that there exists a monotonic relationship between the correlation level (C) of the multi-compartment synaptic input model and modulation depth (α) of the reduced synaptic input model (supporting Fig. S1).

Shape of the selectivity curve

The precise shape and position of the selectivity curve is closely linked to sub-threshold resonance of the TC relay neuron (Hutcheon & Yarom, 2000). Sub-threshold resonance is conveniently examined by driving the membrane with a chirp signal [$g_{GPi\text{-}Th}$ = 0.2 mS/cm^2, α = 0.5, frequency (f_{GPi}) slowly increasing from 0 to 100 Hz] and recording the response of the neuron assessed by the amplitude of the membrane potential of the TC relay neuron (V_m) as a function of input frequency (Fig. 3A and B). Sub-threshold resonance and input selectivity of the TC relay neuron is predominantly dependent on I_T inactivation and membrane time constant, while I_T activation amplifies the response at the resonant frequency (Hutcheon & Yarom, 2000). Resonance frequency and optimum frequency range of the selectivity curve are determined by the inactivation time constant of I_T and the membrane time constant (Hutcheon & Yarom, 2000). Oscillatory GPi input, where frequency of the input corresponds to average GPi bursting frequency, de-inactivates I_T, providing a driving force for depolarization of the TC relay neuron (Golomb *et al.*, 1994, 1996; Destexhe *et al.*, 1996, 1998; Kepecs *et al.*, 2002). GPi burst

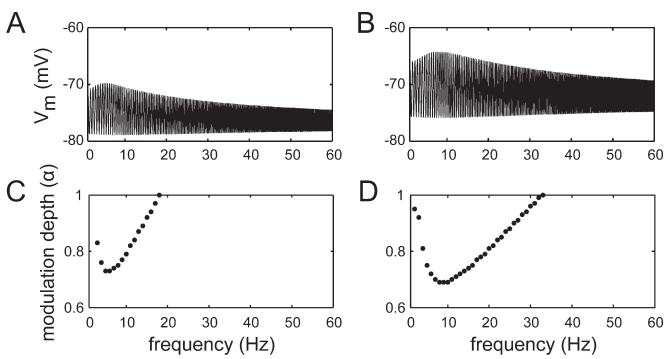

FIG. 3. The relationship between sub-threshold resonance and the selectivity curve. For A and C membrane potential is at the resting membrane potential (−62 mV) and for B and D an additional depolarizing current is injected into the TC relay neuron (I_{app} = −0.6 μA/cm^2). In A and B the membrane is driven with a chirp signal [$g_{GPi\text{-}Th}$ = 0.2 mS/cm^2, α = 0.5, frequency (f_{GPi}) slowly increasing from 0 to 100 Hz]. (A) The limits of sub-threshold membrane oscillation at the resting membrane potential and (B) during depolarizing current injection. (C) The selectivity curve of the TC relay neuron at the resting membrane potential and (D) during depolarizing current injection.

frequencies and modulation depths (correlation levels), chosen above the selectivity curve, give rise to I_{Na} activation and action potential generation at the GPi burst frequency. For oscillatory GPi inputs at frequencies less than the resonance frequency, release of hyperpolarization is sufficiently slow for I_T to inactivate. This reduces the depolarizing drive by I_T and hence prevents action potential generation. Therefore, at low input frequencies, higher modulation depth (correlation level) is required for TC relay neuron to respond to the oscillatory GPi input (Fig. 3C). This effect subsides as the input frequency approaches $1/(2\pi\tau_h)$ where τ_h is the inactivation time constant of I_T (Hutcheon & Yarom, 2000). For oscillatory GPi inputs at frequencies beyond $1/(2\pi\tau_h)$ passive membrane properties begin to influence the response of the TC relay neuron. At GPi oscillation frequencies greater than $1/(2\pi\tau)$, where τ is the membrane time constant, passive membrane properties (i.e. leak conductance and membrane capacitance) attenuate the response of the cell to high-frequency input. As a result, stronger oscillation amplitude, i.e. higher modulation depth (correlation level), is required to drive the TC membrane potential beyond the threshold for action potential generation (Fig. 3C) (Hutcheon & Yarom, 2000). Active and passive properties of the membrane change with the membrane potential, which is directly affected by depolarizing or hyperpolarizing current injection. Depolarizing current injection ($I_{app} = -0.6$ $\mu A/cm^2$) lowers both the inactivation time constant of I_T and the membrane time constant, shifting the resonance frequency and selectivity curve to higher frequencies and lower correlation level or modulation depth values (Fig. 3B and D).

Sensitivity analysis for the selectivity curve in the single-compartment model

We investigated the sensitivity of the selectivity curve to changes in the membrane potential that may result from excitatory and/or inhibitory synaptic background activity. Figure 4 shows how the selectivity curve changes as I_{app} increases from -1.2 to 1.2 $\mu A/cm^2$ (Eqn 2). With increasingly hyperpolarizing current injection ($I_{app} > 0$), the selectivity curve shifted to higher modulation depth values and covered narrower frequency ranges. Also, the optimum frequency range shifted to lower frequencies. By contrast, with increasing depolarizing current ($I_{app} < 0$), the selectivity curve shifted to lower modulation depth values and covered higher frequency ranges. Thus, dependent on the synaptic background activity, TC relay neurons preferentially relay the frequency content of the synchronized drive from GPi neurons exhibiting burst activity at a frequency located in the range 2–25 Hz. Such oscillations in the GPi have been observed experimentally (Brown, 2003).

Effect of inhibitory input selectivity on TC relay function in the single-compartment model

We next investigated the TC relay function in the presence of an excitatory cortical input and various states of GPi input (i.e. uncorrelated, correlated, bursting, etc.) by monitoring the frequency content of the TC relay neuron's output patterns using the single-compartment TC relay neuron model. In the absence of correlated GPi bursting ($\alpha = 0$), the TC relay neuron faithfully relayed the excitatory cortical input, as evidenced by the presence of a single peak centred at the cortical input frequency in the TC cell's output spectrum [Fig. 5A (time signal) and 5D (Fourier transform of the signal)]. For correlated GPi input parameters chosen below the selectivity curve (Fig. 4), the GPi bursting frequency appears in the output spectrum but the overall signal is still dominated by the frequency components corresponding to the excitatory cortical input (Fig. 5E). By contrast, for GPi input parameters chosen above the selectivity curve (Fig. 4), the primary frequency component of the TC neuron's output shifted from the excitatory cortical input frequency to the inhibitory GPi bursting frequency (Fig. 5F).

Section B: TC frequency selectivity during DBS

Effect of STN-DBS frequency and stimulus amplitude

We investigated the effects of STN-DBS on the TC relay neuron by implementing the BG network model of Rubin & Terman (2004)

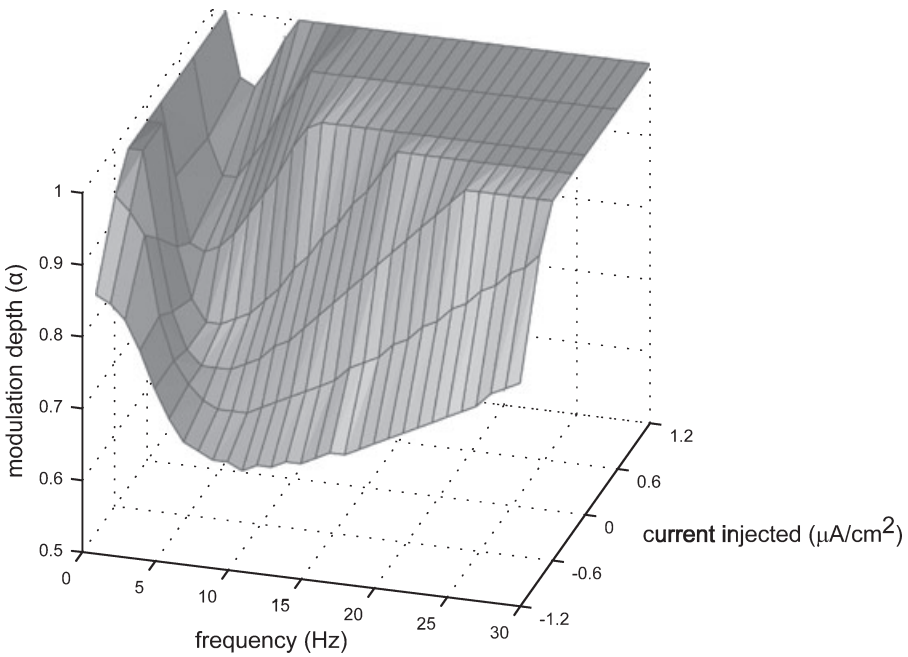

FIG. 4. Sensitivity analysis of the selectivity curve during constant hyperpolarizing or depolarizing current injection representing background synaptic activity. Shape of the selectivity curve and position of the optimum frequency range are defined by the passive and active properties of the membrane, which are in turn dependent on the TC relay neuron's membrane potential. During constant hyperpolarizing current injection ($I_{app} > 0$), the selectivity curve shifts to lower frequencies and higher modulation depth values. By contrast, during constant depolarizing current injection ($I_{app} < 0$), the selectivity curve shifts to higher frequencies and lower modulation depth values ($g_{GPi\text{-}Th} = 0.2$ mS/cm^2).

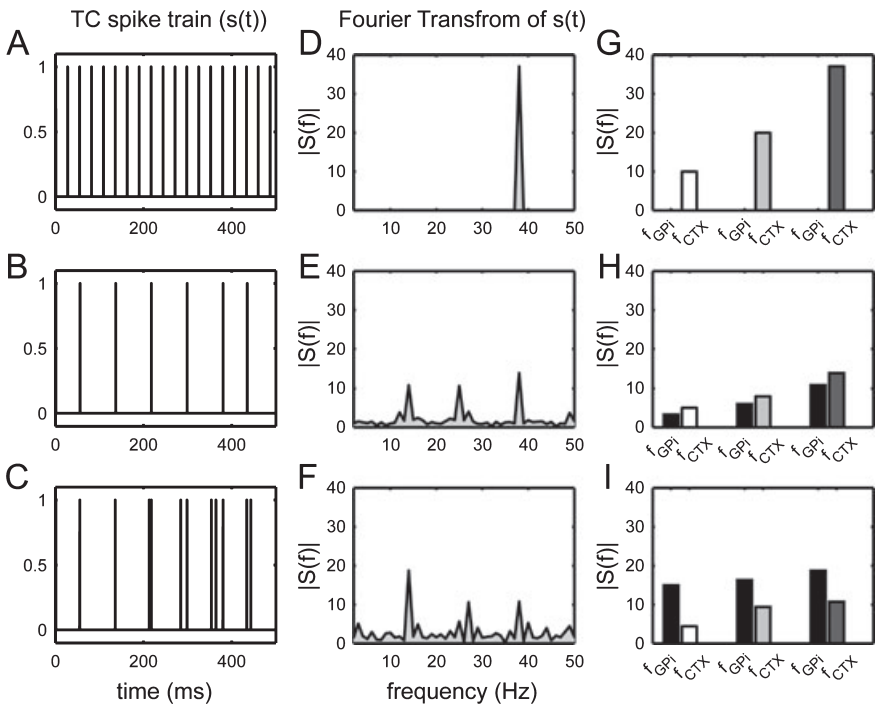

FIG. 5. Relationship between TC relay neuron's inhibitory input selectivity and relay function. Spike trains obtained from the TC relay neuron [s(t)] are shown in A–C and Fourier transforms of the spike trains [S(f)] are shown in D–F. Magnitude of GPi burst frequency [f_{GPi} = 13 Hz (black bar)] and cortical frequency in the TC output for various cortical frequencies are shown in G–I [f_{CTX} = 10 Hz (white bar), f_{CTX} = 20 Hz (light gray bar) and f_{CTX} = 37 Hz (dark grey bar)]. For G–I, differences between cortical frequency magnitudes in the TC output is a direct consequence of the Fourier transform. A, D and G: for uncorrelated GPi input (i.e. $\alpha = 0$) TC neuron only relays cortical input frequency; B, E and H: for GPi input parameters chosen below the selectivity curve (Fig. 3C), TC neuron relays GPi burst frequency together with the cortical input frequency, the predominant component being the cortical input frequency; C, F and I: for correlated oscillatory GPi input parameters chosen above the selectivity curve (Fig. 3C), TC neuron relays GPi burst frequency together with the cortical input frequency, the predominant component being the GPi burst frequency (g_{CTX} = 0.2 mS/cm^2, δ_{CTX} = 1.5 ms, $g_{GPi\text{-}Th}$ = 0.2 mS/cm^2, f_{GPi} = 13 Hz).

(Fig. 1). Rubin & Terman (2004) assume 100% activation of STN neurons and refer to pulse amplitude as the amplitude of current injected into the STN neurons during DBS (i.e. $i_D > 0$ and the same for all STN neurons during DBS). In order to investigate the effects of both DBS frequency and stimulus amplitude on the TC relay neuron, we assume a monotonic relationship between stimulus amplitude and the percentage of STN neurons activated by DBS (Butson and McIntyre, 2005; Butson *et al*., 2007). The percentage of STN neurons activated by DBS is equivalent to the percentage of neurons receiving non-zero current injection due to DBS ($i_D > 0$); by contrast, for the neurons which are not activated, i_D is set at 0.

DBS induces high-frequency tonic activity in STN, GPe and GPi neurons and the percentage of GPe and GPi neurons activated is monotonically related to the percentage of STN neurons activated. The monotonic relationship between the percentage of GPi and GPe neurons activated with respect to the percentage of STN neurons activated is dependent on the network connectivity. STN, GPe and GPi neurons, which are not relaying high-frequency tonic activity, continue to exhibit synchronized bursting activity driven by the hyper-direct pathway. Figure 6 demonstrates activity patterns exhibited by a GPi neuron when it is activated by STN-DBS (Fig. 6A and C) and when it is bursting at 15 Hz due to the influence of the oscillatory hyper-direct pathway ($f_{CTX\text{-}STN}$ = 15 Hz) (Fig. 6B and D).

In order to study effects of DBS stimulus amplitude on the relay properties of the TC relay neuron, we varied the percentage of STN neurons activated for a given DBS frequency. As the percentage of STN neurons activated increased, the magnitude of GPi burst frequencies in the TC output decreased (Fig. 7A and B). We repeated the same analysis in the presence of cortical input to the TC relay neuron, and observed that GPi burst frequencies were suppressed as the percentage of STN neurons activated increased while cortical input frequencies were not affected (Fig. 7C and D).

We next determined which DBS parameters resulted in significant suppression of GPi burst frequencies in TC output. Significant suppression is defined as greater than 50% reduction in the magnitude of GPi burst frequencies with respect to magnitude of GPi burst frequencies in the absence of DBS. Figure 8 shows the boundary between relay of GPi burst frequencies and suppression (65 and 100%) of GPi burst frequencies in TC output. There is an inverse relationship between DBS frequency and the percentage of STN neurons that need to be activated in order to suppress GPi burst frequencies in TC output. Figure 7A and B are particular examples from Figure 8 and qualitatively represent the frequency content of the TC output during STN-DBS with parameters chosen below the inverse relationship and above the inverse relationship. For 100% suppression of GPi burst frequencies, DBS frequency should be greater than or equal to 60 Hz. DBS frequencies less than 60 Hz were not effective in 100% suppression of GPi burst frequencies as low-frequency DBS was not as effective as high-frequency DBS in regularizing oscillatory BG activity patterns (Rubin & Terman, 2004). We repeated the same analysis in the presence of cortical input and observed that the inverse relationship between DBS frequency and percentage of STN neurons activated holds. In the presence of cortical input, it was not possible to suppress fully (i.e. 100%) GPi burst frequencies in the TC output due to aliasing between multiple frequencies input into the system.

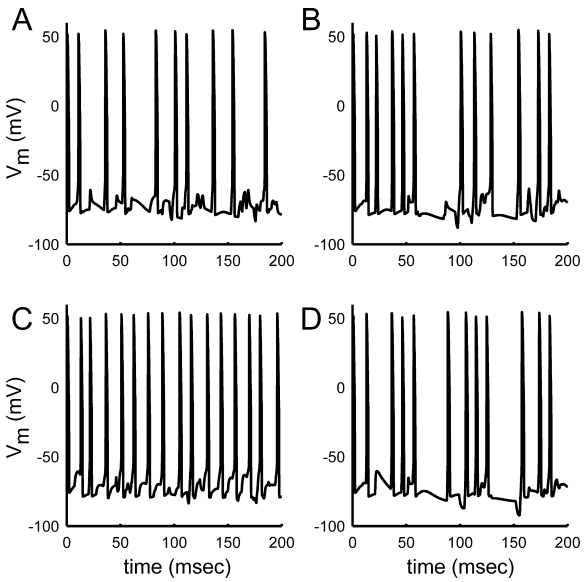

FIG. 6. (A) Activity pattern of a GPi neuron activated during STN-DBS at 40 Hz. (B) Activity pattern of a GPi neuron bursting at 15 Hz during STN-DBS at 40 Hz. (C) Activity pattern of a GPi neuron activated during STN-DBS at 130 Hz. (D) Activity pattern of a GPi neuron bursting at 15 Hz during STN-DBS at 130 Hz. High-frequency DBS is more effective in regularizing GPi activity patterns than low-frequency DBS.

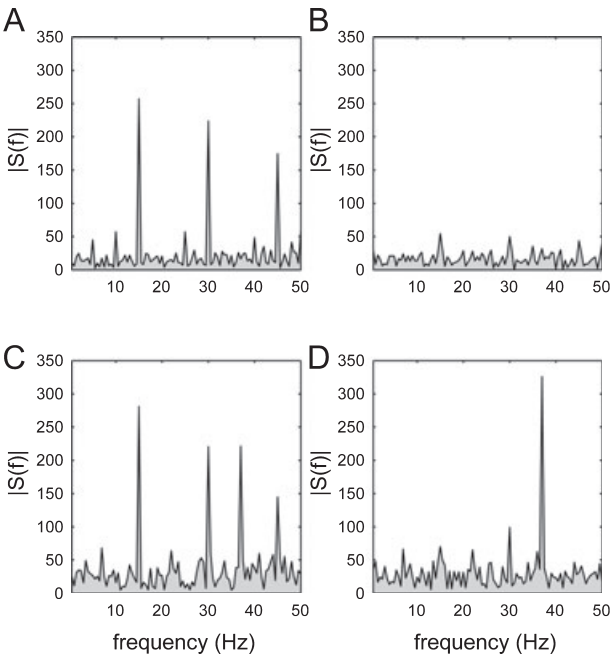

FIG. 7. As the percentage of STN neurons activated by DBS increases from 0 to 100%, the magnitude of GPi burst frequency in the TC output decreases. Total number of STN neurons included in the network model is 16 and average GPi burst frequency is 15 Hz. Fourier transform of the spike trains obtained from the TC relay neuron [S(f)] (A) during STN-DBS at 110 Hz when 12.5% of STN neurons are activated by DBS and (B) when 31.25% of STN neurons are activated by DBS; Fourier transform of the spike trains obtained from the TC relay neuron [S(f)] in the presence of cortical input (C) when the frequency of DBS is 110 Hz and 12.5% of STN neurons are activated and (D) when 31.25% of STN neurons are activated. In the presence of an excitatory cortical input to the TC relay neuron, as the percentage of STN neurons activated by DBS increases, relay of the cortical input is restored due to suppression of GPi burst frequencies, which can be as strong as the magnitude of cortical frequencies in the TC output (for C and D f_{CTX} = 37 Hz, g_{CTX} = 0.2 mS/cm^2, δ_{CTX} = 5 ms).

The inverse relationship between DBS frequency and percentage of STN neurons activated is based on an intricate interaction between network properties and the membrane properties of TC relay neurons.

Network properties contributing to the inverse relationship

As the percentage of STN neurons activated by DBS increases, the magnitude of GPi burst frequencies decrease in the summed synaptic input from GPi neurons to the TC relay neuron (Fig. 9). Simultaneously, the DC component, which corresponds to the mean of the summed synaptic conductance, and DBS induced an increase in the high-frequency component (Fig. 9). Changes in the magnitude of different frequencies expressed in the summed synaptic output are dependent on the percentage of STN neurons activated by DBS and the DBS frequency (Fig. 9).

Modulation depth approximates temporal changes in the summed synaptic input from GPi neurons and this approximation is well defined when the number of pre-synaptic neurons is large (i.e. greater than 100) (Section A). The network model includes 16 GPi neurons. Therefore, temporal changes in the summed synaptic input cannot be quantified by modulation depth changes. However, changes occurring in the summed synaptic input can be related to changes in the modulation depth through the magnitude of GPi burst frequency.

With respect to the magnitude of GPi burst frequency in the absence of DBS (2×10^4), a reduction in the magnitude of GPi burst frequency during DBS at 50 Hz is analogous to reducing the modulation depth from 0.85 (12.5% STN neurons activated) to 0.25 (62.5% STN neurons activated). By contrast, during DBS at 110 Hz, reduction in the magnitude of GPi burst frequency is comparable to reducing the modulation depth from 0.75 (when 12.5% of STN neurons are activated) to 0.15 (when 62.5% of STN neurons are activated).

Cellular properties contributing to the inverse relationship

In addition to the changes in the overall BG output profile, the membrane properties of the TC relay neurons also contribute to the inverse relationship. As described in Section A, oscillatory GPi input gives rise to de-inactivation of I_T, which provides a depolarizing drive to the TC relay neuron (Golomb *et al.*, 1994, 1996; Destexhe *et al.*, 1996, 1998; Kepecs *et al.*, 2002). For GPi inputs within the TC relay neuron's selectivity window, this depolarizing drive recruits I_{Na}, leading to action potential generation at the GPi burst frequency (Fig. 10). Action potential generation at the GPi burst frequency occurs only during a narrow time window (Fig. 10). During DBS, the high-frequency component of the GPi input periodically hyperpolarizes the TC relay neuron. If the DBS-induced high-frequency component of the GPi input coincides with this time window, action potential generation is disrupted (Fig. 10).

Discussion

A computational model was used to investigate the neuronal basis of DBS as it is used for the treatment of PD. First, the response of a TC relay neuron to correlated GPi input in the theta and beta band was studied in order to determine the changes in thalamic functionality during PD. The effects of STN-DBS on TC information processing were investigated next and we focused particularly on the inverse

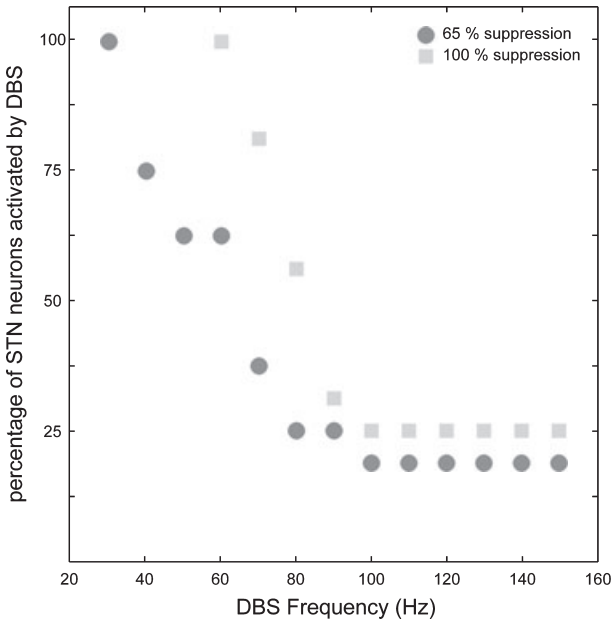

FIG. 8. Inverse relationship between DBS frequency and percentage of STN neurons activated required to suppress relay of GPi burst frequencies. As the frequency of DBS decreases, more STN neurons need to be activated by DBS in order to suppress GPi burst frequencies in the TC output. The data points (indicated by squares and circles) separate relay of the GPi bursting to CTX from significant suppression of GPi burst frequencies in the TC output. The amount of GPi burst frequency suppression is computed with respect to GPi burst frequency in the TC output in the absence of DBS. The 65% and 100% suppression levels are chosen as examples to illustrate the changes which occur in the inverse relationship for different suppression levels.

relationship that has been observed between clinically effective DBS frequency and amplitude (Benabid *et al.*, 1991; Gao *et al.*, 1999; Rizzone *et al.*, 2001; Moro *et al.*, 2002). The main findings are as follows. (i) The TC relay neuron selectively responds to highly synchronized GPi inputs bursting at a frequency located in the range 2–25 Hz. When the TC relay neuron responds to the GPi input, the GPi burst frequencies are introduced in the TC output while simultaneously relay of excitatory cortical input is suppressed. (ii) DBS with sufficient frequency and amplitude suppresses relay of pathological GPi-induced frequencies to CTX. (iii) The model provides an explanation for the clinically observed inverse relationship between DBS amplitude and frequency based on the cellular dynamics of TC relay neurons.

To investigate the response of a TC relay neuron to correlated GPi input, we have used two different TC relay neuron models, one computationally intensive multi-compartment model with realistic morphology and multi synaptic input and one single-compartment model with collapsed morphology and simplified synaptic input, capable of capturing in its modulation depth the essence of the correlated GPi input. In this way we were able to validate the single-compartment model against the detailed multi-compartment one, which enabled us to utilize the computationally less intensive single-compartment model for performing specific analyses in large parameter spaces (e.g. Figs 4 and 8). To investigate the effects of DBS on the TC relay neuron, a BG network model has been utilized (Rubin & Terman, 2004; Pirini *et al.*, 2009). The network model consists of 16 STN, 16 GPe and 16 GPi neurons. Use of this model has enabled us to study the interactions within the BG network resulting from STN-DBS and to investigate the effects of altered GPi output on the TC relay neuron. The changes we observe in BG output during STN-DBS and the consequences on TC relay function are analogous to effects of correlation level and modulation depth changes studied in Section A.

We did not observe mismatch between the multi-compartment and single-compartment TC relay neuron models for the properties that we highlight here, suggesting that the main mechanism dictating TC input frequency selectivity is not strongly dependent on the dendritic structure but is rather based on more fundamental membrane properties and ion-channel dynamics. Simulations revealed that correlated low-frequency GPi input induced action potentials at the GPi burst frequency while high-frequency input patterns did not lead to a response. The GPi input burst frequency range which the TC relay neuron selectively responds to is approximately 2–25 Hz (depending on membrane potential). Such frequencies have been recorded experimentally during PD and associated with PD motor symptoms (Nini *et al.*, 1995; Magnin *et al.*, 2000; Raz *et al.*, 2000; Brown *et al.*, 2001). Our simulations also highlight that GPi burst frequency is not the only key determinant of TC relay neuron response. Input correlation level also dictates how the TC relay neuron responds to the synaptic input. It has been shown that correlation levels among GPi neurons increase during PD (Raz *et al.*, 2000).

In agreement with earlier studies (Rubin & Terman, 2004; Guo *et al.*, 2008) we observed that for phasic GPi inputs the relay of

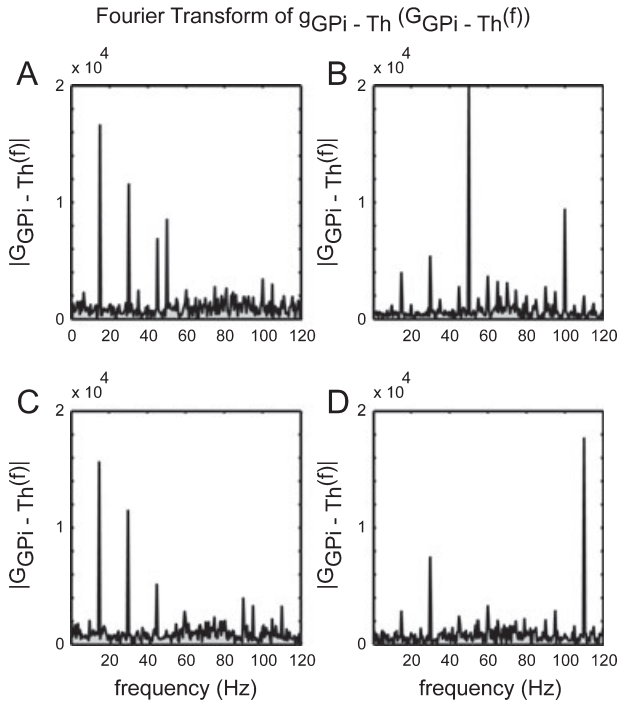

FIG. 9. Variations in the frequency content of the summed GPi input to the TC relay neuron ($g_{GPi\text{-}Th}$) for different DBS frequencies and percentages of STN neurons activated. Frequency spectrum of the summed GPi input to TC relay neuron is obtained using a Fourier transform [$G_{GPi\text{-}Th}(f)$] (the DC component of the frequency spectrum is removed for ease of visualization). As the percentage of STN neurons activated by DBS increases, GPi bursting frequency decreases while the constant inhibition applied to TC relay neuron increases (the DC component of the frequency spectrum). A and B: frequency of DBS is 50 Hz. As the percentage of STN neurons activated increased from 12.5 to 62.5%, the DC component of the frequency spectrum increased from 5.75×10^4 to 9×10^4 and the magnitude of GPi burst frequency decreased from 1.7×10^4 to 5×10^3. C and D: frequency of DBS is 110 Hz. As the percentage of STN neurons activated increased from 12.5 to 62.5%, the DC component of the frequency spectrum increased from 5.9×10^4 to 9.75×10^4 and the magnitude of GPi burst frequency decreased from 1.56×10^4 to 2.8×10^3.

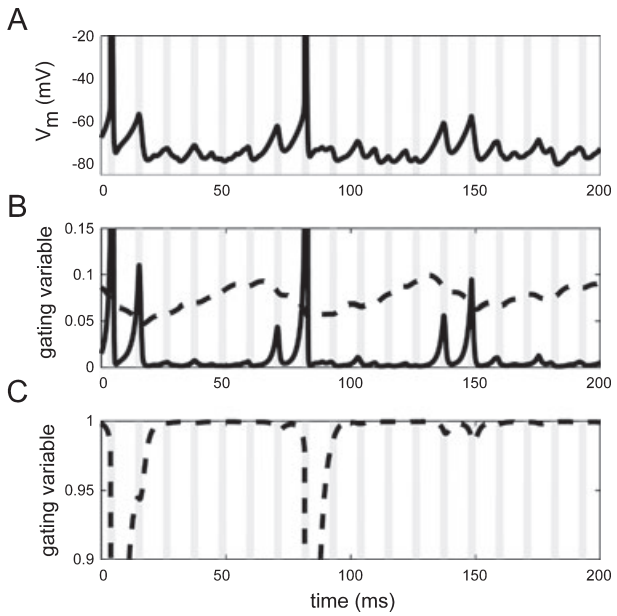

FIG. 10. TC cellular properties contributing to the inverse relationship between percentage of STN neurons activated and DBS frequency required to suppress relay of GPi burst frequencies. Grey bars indicate the onset and duration of DBS pulses (Eqn 8). (A) Membrane potential of the TC relay neuron during DBS of 90 Hz when 31.25% of the STN neurons were activated. High-frequency component of the GPi output driven by DBS periodically hyperpolarizes the TC relay neuron. In B, the dashed line depicts I_T, the inactivation gating variable, while the solid line corresponds to I_{Na} activation; in C, the dashed line corresponds to I_{Na}, the inactivation gating variable. Periodic hyperpolarization of the membrane disrupts I_{Na} influx and prevents action potential generation if brief hyperpolarization occurs at the right time (e.g. as shown at 150 ms).

excitatory cortical inputs by TC relay neurons becomes impaired. We have studied the relay of excitatory cortical inputs using the single-compartment model. Therefore, intricate details of the excitatory and inhibitory synaptic interactions in the dendritic tree have not been taken into account. We have chosen to study frequency components of the TC output as a measure for TC functionality instead of the 'error – index' analysis introduced by Rubin & Terman (2004). 'Error – index' analysis provides information regarding how well the TC neuron relays an excitatory input to CTX while spectral analysis provides insight about the temporal content of the TC output, enabling assessment of the relative contribution of GPi and cortical frequencies to the TC output. Moreover, use of spectral analysis as a measure of TC functionality provided a clear link to several clinical studies which have highlighted the relationship between emergence and alleviation of PD motor symptoms and frequencies observed in BG (Chen *et al.*, 2006, 2007; Fogelson *et al.*, 2005; Hutchison *et al.*, 2004; Levy *et al.*, 2000, 2002; Trottenberg *et al.*, 2007; Brown *et al.*, 2001, 2004; 2005; Hammond *et al.*, 2007).

We observed that the magnitude of GPi burst frequency increased in the TC output, with increasingly correlated GPi drive. Simultaneously, the magnitude of frequencies related to the relay of cortical information decreased with the appearance of GPi burst frequencies in the TC output. These findings support the hypothesis that thalamus transmits synchronized BG oscillations to CTX during PD (Brown, 2003). We observed that under 'PD conditions', the TC relay neuron switches to a regime where the oscillatory drive from GPi is transmitted into the cortico-thalamic loop. This suggests a mechanism through which low-frequency BG oscillations, via thalamus, result in synchronization of the motor CTX at anti-kinetic low frequencies during PD (Brown, 2003; Hammond *et al.*, 2007).

Rubin & Terman (2004) pointed out that regularization of BG output through DBS-induced high-frequency activity may restore TC relay functionality. In their model, it is assumed that DBS replaces all oscillatory activity in STN and hence excludes effects of stimulus amplitude from the analysis and provides a possible mechanism for DBS efficacy based on DBS frequency. Under the assumption that DBS replaces all oscillatory activity, DBS restores TC relay functionality by replacing phasic inhibition of TC relay neurons (DBS off) with constant inhibition (DBS on) (Rubin & Terman, 2004).

Based on modelling studies demonstrating that there exists a monotonic relationship between DBS stimulus amplitude and the size of the activation field of the electrode, we included a DBS stimulus amplitude-dependent activation of STN (Butson & McIntyre, 2005; Butson *et al.*, 2007). The assumption that DBS does not replace all oscillatory synchronous activity in the BG is also supported by clinical observations indicating that for therapeutic stimulation frequencies and sub-therapeutic stimulus amplitudes, PD motor symptoms are still present (Rizzone *et al.*, 2001; Moro *et al.*, 2002).

Brown (2003) categorized frequency bands of oscillation in the BG as anti-kinetic (oscillation frequencies in the theta and beta bands) and pro-kinetic (oscillation frequencies in the high gamma band) based on their net effect on movement. Our simulations indicate that DBS stimulus amplitude, which is monotonically related to the percentage of STN neurons activated, predominantly dictates the balance between anti-kinetic low-frequency and pro-kinetic high-frequency activity patterns in the BG network (Brown, 2003; Hahn *et al.*, 2008). We observe suppression of anti-kinetic frequencies in TC output for certain DBS frequencies and percentage of STN neurons activated which are inversely related to one another (Fig. 8) (Brown *et al.*, 2001, 2004; Hammond *et al.*, 2007). There exists a minimum activation level of STN neurons below which suppression of anti-kinetic low frequencies in the TC output does not occur independent of DBS frequency, which is in line with clinical observations of a DBS stimulus amplitude threshold for therapeutic efficacy (Moro *et al.*, 2002). By contrast, DBS frequency affects both the content of the high-frequency activity patterns in the BG network and the cellular dynamics of the TC relay neuron. For instance, for DBS frequencies less than 60 Hz, STN, GPe and GPi neurons carry both the DBS-induced high-frequency and anti-kinetic low-frequency activity patterns even during 100% activation of STN neurons. At these DBS frequencies, 100% suppression of anti-kinetic frequencies in the TC output is not possible, indicating that there exists a minimum DBS frequency below which a given level of anti-kinetic frequency suppression cannot be achieved.

It remains unknown why relatively high-frequency stimulation (e.g. 130 Hz) is required for clinical efficacy of DBS (Benabid *et al.*, 1991; Moro *et al.*, 2002). The modelling work presented in the present study suggests three potential mechanisms which could play a role in the efficacy of high-frequency stimulation: (i) high-frequency DBS is more effective in suppressing anti-kinetic low frequencies in the BG output; (ii) high-frequency DBS gives rise to increased constant inhibition of the TC relay neuron, reducing the region where the TC neuron selectively relays inhibitory oscillatory inputs at anti-kinetic low frequencies; and (iii) the probability that relay of anti-kinetic frequencies is suppressed by DBS-induced inhibitory post-synaptic potentials in TC is proportional to DBS frequency. We explain these mechanisms in more detail below.

DBS suppresses anti-kinetic frequencies in the TC output by altering the BG output and affecting the cellular dynamics of the TC

relay neuron. STN-DBS alters the BG output by introducing high-frequency tonic (regular) activity in the BG output. Changes in the BG output are proportional to the fraction of STN neurons activated and the frequency of DBS. During DBS, the BG output consists of two distinct activity patterns: an anti-kinetic oscillatory component and high-frequency regular component induced by DBS (Fig. 9). As the percentage of STN neurons activated increases, the magnitude of anti-kinetic oscillation frequencies decreases in the BG output while simultaneously the average level of inhibition applied to the TC relay neuron increases (Rubin & Terman, 2004). Application of constant hyperpolarization shifts the selectivity curve of the TC relay neuron to lower GPi burst frequencies and higher modulation depths (Fig. 4). As a result, the pre-synaptic frequency–amplitude window to which TC relay neurons selectively respond to shrinks as the number of STN neurons activated by DBS increases. Additionally, the DBS-induced high-frequency component of the BG output briefly hyperpolarizes the TC relay neuron at regular intervals. Based on the assumption that DBS does not fully replace anti-kinetic frequencies in the BG output, the TC relay neuron can still fire action potentials at these frequencies (Fig. 10). Regular inhibitory post-synaptic potentials induced by DBS interfere with action potential generation due to oscillatory BG input and further suppress anti-kinetic frequencies in the TC output (Fig. 10). The frequency of DBS directly controls the probability of the inhibitory post-synaptic potentials occurring at the right time and is therefore more effective than low-frequency DBS.

It is remarkable that relay of cortical frequencies is far more robust to the presence of DBS than relay of BG oscillation frequencies (Fig. 7C and D). The time window during which action potentials are generated due to the cortical input is an order of magnitude shorter than the time window during which action potentials are generated because of the oscillatory BG input. Action potential generation driven by the cortical input can be temporarily suppressed only in the case of perfect alignment of an inhibitory post-synaptic potential induced by DBS with the cortical input. As a result, the magnitude of cortical frequencies in the TC output remains on average constant while BG oscillation frequencies are effectively suppressed during DBS. In the absence of DBS, anti-kinetic frequencies can be expressed as strongly as the cortical frequencies in the TC output. With increasing percentage of STN neurons activated during DBS, relay of cortical frequencies is restored as a result of suppression of these anti-kinetic frequencies in the TC output (Fig. 7D).

Supporting information

Additional supporting information may be found in the online version of this article:

Fig. S1. Derivation of the reduced synaptic input.

Please note: as a service to our authors and readers, this journal provides supporting information supplied by the authors. Such materials are peer-reviewed and may be re-organized for online delivery, but are not copy-edited or typeset by Wiley-Blackwell. Technical support issues arising from supporting information (other than missing files) should be addressed to the authors.

Acknowledgements

We thank Kevin Dolan and Michel Decré for fruitful discussions. H.C. is a Marie Curie Fellow of the European Community (MEST-CT-2004-007832).

Abbreviations

BG, basal ganglia; CTX, cortex; DBS, deep brain stimulation; GPe, globus pallidus externum; GPi, globus pallidus internum; PD, Parkinson's disease; STN, subthalamic nucleus; TC, thalamocortical; Th, thalamus.

References

Baufreton, J., Atherton, J.F., Surmeier, D.J. & Bevan, M.D. (2005) Enhancement of excitatory synatpic integration by GABAergic inhibition in the subthalamic nucleus. *J. Neurosci.*, **25**, 8505–8517.

Benabid, A.L. (2003) Deep brain stimulation for Parkinson's disease. *Curr. Opin. Neurobiol.*, **13**, 696–706.

Benabid, A.L., Pollak, P., Gervason, C., Hoffman, D., Gao, D.M., Hommel, M., Perret, J.E. & Rougemont, J.D. (1991) Long-term suppression of tremor by chronic stimulation of the ventral intermediate thalamic nucleus. *Lancet*, **337**, 403–406.

Beurrier, C., Bioulac, B., Audin, J. & Hammond, C. (2001) High frequency stimulation produces a transient blockade of voltage gated currents in subthalamic neurons. *J. Neurophysiol.*, **85**, 1351–1356.

Brown, P. (2003) The oscillatory nature of human basal ganglia activity: relationship to pathophysiology of Parkinson's disease. *Mov. Disord.*, **18**, 357–363.

Brown, P. & Williams, D. (2005) Basal ganglia local field potential activity: character and functional significance in the human. *Clin. Neurophysiol.*, **116**, 2510–2519.

Brown, P., Oliviero, A., Mazzone, P., Insola, A., Tonali, P. & Lazzaro, V.D. (2001) Dopamine dependency of oscillations between subthalamic nucleus and pallidum in Parkinson's disease. *J. Neurosci.*, **21**, 1033–1038.

Brown, P., Mazzone, P., Oliviero, A., Altibrandi, M.G., Pilato, F., Tonali, P.A. & Lazzaro, V.D. (2004) Effects of stimulation of the subthalamic area on oscillatory pallidal activity in Parkinson's disease. *Exp. Neurol.*, **188**, 480–490.

Butson, C.R. & McIntyre, C.C. (2005) Tissue and electrode capacitance reduce neural activation volumes during deep brain stimulation. *Clin. Neurophsiol.*, **116**, 2490–2500.

Butson, C.R., Cooper, S.E., Henderson, J.M. & McIntyre, C.C. (2007) Patient specific analysis of the volume of tissue activated during deep brain stimulation. *NeuroImage*, **34**, 661–670.

Chen, C.C., Pogostan, A., Zrinzo, L.U., Tisch, S., Limousin, P., Ashkan, K., Yousry, T., Hariz, M.I. & Brown, P. (2006) Intra-operative recordings of local field potentials can help localize the subthalamic nucleus in Parkinson's disease surgery. *Exp. Neurol.*, **198**, 214–221.

Chen, C.C., Litvak, V., Gilbertson, T., Kuhn, A., Lu, C.S., Lee, S.T., Tsai, C.H., Tisch, S., Limousin, P., Hariz, M. & Brown, P. (2007) Excessive synchronization of basal ganglia neurons at 20 Hz slows movement in Parkinson's disease. *Exp. Neurol.*, **205**, 214–221.

Destexhe, A. & Sejnowski, T.J. (2003) Interactions between membrane conductances underlying thalamocortical slow-wave oscillations. *Phys. Rev.*, **83**, 1401–1453.

Destexhe, A., Contreras, D., Steriade, M., Sejnowski, T.R. & Huguenard, J.R. (1996) In vivo, in vitro and computational analysis of dendritic calcium currents in thalamic reticular neurons. *J. Neurosci.*, **16**, 169–185.

Destexhe, A., Neubig, M., Ulrich, D. & Huguenard, J. (1998) Dendritic low threshold calcium currents in thalamic relay cells. *J. Neurosci.*, **18**, 3574–3588.

Dostrovsky, J.O. & Lozano, A.M. (2002) Mechanisms of deep brain stimulation. *Mov. Disord.*, **17**, 63–68.

Fogelson, N., Kuhn, A.A., Silberstein, P., Limousin, P.D., Hariz, M., Trottenberg, T., Kupsch, A. & Brown, P. (2005) Frequency dependent effects of subthalamic nucleus stimulation in Parkinson's disease. *Neurosci. Lett.*, **382**, 5–9.

Gao, D.M., Benazzouz, A., Piallat, B., Bressand, K., Ilinsky, I.A., Kultas-Ilinsky, K. & Benabid, A.L. (1999) High frequency stimulation of the subthalamic nucleus suppresses experimental resting tremor in the monkey. *Neuroscience*, **88**, 201–212.

Golomb, D., Wang, X.J. & Rinzel, J. (1994) Synchronization properties of spindle oscillations in a thalamic reticular nucleus model. *J. Neurophysiol.*, **72**, 1109–1126.

Golomb, D., Wang, X.J. & Rinzel, J. (1996) Propagation of spindle waves in a thalamic slice model. *J. Neurophysiol.*, **75**, 750–769.

Guo, Y., Rubin, J.E., McIntyre, C.C., Vitek, J.L. & Terman, D. (2008) Thalamocortical relay fidelity varies across subthalamic nucleus deep brain stimulation protocols in a data driven computational model. *J. Neurophysiol.*, **99**, 1477–1492.

Hahn, P. J., Russo, G. S., Hashimoto, T., Miocinovic, S., Xu, W., McIntyre, C. C. & Vitek, J. L. (2008) Pallidal burst activity during therapeutic deep brain stimulation. *Exp. Neurol.*, **211**, 243–251.

Hammond, C., Bergman, H. & Brown, P. (2007) Pathological synchronization in Parkinson's disease: networks, models and treatments. *Trends Neurosci.*, **30**, 357–364.
Hashimoto, T., Elder, C.M., Okun, M.S., Patrick, S.K. & Vitek, J.L. (2003) Stimulation of the subthalamic nucleus changes the firing pattern of pallidal neurons. *J. Neurosci.*, **23**, 1916–1923.
Hines, M.L. & Carnevale, N.T. (1997) The NEURON simulation environment. *Neural Comput.*, **9**, 1179–1209.
Holsheimer, J. (2002) Which neuronal elements are activated directly by spinal cord stimulation. *Neuromodulation*, **5**, 25–31.
Huguenard, J.R. & McCormick, D.A. (1992) Simulation of the currents involved in rhythmic oscillations in thalamic relay neurons. *J. Neurophysiol.*, **68**, 1373–1383.
Huguenard, J.R. & Prince, D.A. (1992) A novel T-type current underlies prolonged calcium-dependent burst firing in GABAergic neurons of rat thalamic reticular nucleus. *J. Neurosci.*, **12**, 3804–3817.
Hutcheon, B. & Yarom, Y. (2000) Resonance, oscillation and the intrinsic frequency preferences of neurons. *Trends Neurosci.*, **23**, 216–222.
Hutchison, W.D., Dostrovsky, J.O., Walters, J.R., Courtemanche, R., Boraud, T., Goldberg, J. & Brown, P. (2004) Neuronal oscillations in the basal ganglia and movement disorders: evidence form whole animal and human recordings. *J. Neurosci.*, **24**, 9240–9243.
Kepecs, A., Wang, X.J. & Lisman, J. (2002) Bursting neurons signal input slope. *J. Neurosci.*, **22**, 9053–9062.
Kim, U., Sanchez-Vives, M.V. & McCormick, D.A. (1997) Functional dynamics of GABAergic inhibition in the thalamus. *Science*, **278**, 130–134.
Levy, R., Hutchinson, W.D., Lozano, A.M. & Dostrovsky, J.O. (2000) High frequency synchronization of neuronal activity in the subthalamic nucleus of Parkinsonian patients with limb tremor. *J. Neurosci.*, **20**, 7766–7775.
Levy, R., Ashby, P., Hutchinson, W.D., Lang, A.E., Lozano, A.M. & Dostrovsky, J.O. (2002) Dependence of subthalamic nucleus oscillations on movement and dopamine in Parkinson's disease. *Brain*, **125**, 1196–1209.
Lozano, A.M., Dostrovsky, J.O., Chen, R. & Ashby, P. (2002) Deep brain stimulation for Parkinson's disease: disrupting the disruption. *Lancet Neurol.*, **1**, 225–231.
Magnin, M., Morel, A. & Jeanmonod, D. (2000) Single-unit analysis of the pallidum, thalamus, and subthalamic nucleus in parkinsonian patients. *Neuroscience*, **96**, 549–564.
McCormick, D.A. & Huguenard, J.R. (1992) A model of the electrophysiological properties of thalamocortical relay neurons. *J. Neurophysiol.*, **68**, 1384–1400.
McFarland, N.R. & Haber, S.N. (2002) Thalamic relay nuclei of the basal ganglia form both reciprocal and nonreciprocal cortical connections, linking multiple frontal cortical areas. *J. Neurosci.*, **22**, 8117–8132.
McIntyre, C.C., Grill, W.M., Sherman, D.L. & Thakor, N.V. (2004) Cellular effects of deep brain stimulation: model-based analysis of activation and inhibition. *J. Neurophysiol.*, **91**, 1457–1469.
Miocinovic, S., Parent, M., Butson, C.R., Hahn, P.J., Russo, G.S., Vitek, J.L. & McIntyre, C.C. (2006) Computational analysis of subthalamic nucleus and lenticular fasciculus activation during therapeutic deep brain stimulation. *J. Neurophysiol.*, **96**, 1569–1580.
Moro, E., Esselink, R.J.A., Xie, J., Hommel, M., Benabid, A.L. & Pollak, P. (2002) The impact on Parkinson's disease of electrical parameter settings in STN stimulation. *Neurology*, **59**, 706–713.
Nini, A., Feingold, A., Slovin, H. & Bergman, H. (1995) Neurons in the globus pallidus do not show correlated activity in the normal monkey, but phase-locked oscillations appear in the MPTP model of parkinsonism. *J. Neurophysiol.*, **74**, 1800–1805.
Pirini, M., Rocchi, L., Sensi, M. & Chiari, L.A. (2009) Computational modelling approach to investigate different targets in deep brain stimulation for Parkinson's disease. *J. Comput. Neurosci.*, **26**, 91–107.
Raz, A., Vaadia, E. & Bergman, H. (2000) Firing patterns and correlations of spontaneous discharge of pallidal neurons in the normal and tremulous 1-methyl-4-phenyl-1, 2, 3, 6 tetrahydropyridine vervet model of Parkinsonism. *J. Neurosci.*, **20**, 8559–8571.
Rhodes, P.A. & Llinas, R. (2005) A model of thalamocortical relay cells. *J. Physiol.*, **565**, 765–781.
Rizzone, M., Lanotte, M., Bergamasco, B., Tavella, A., Torre, E., Faccani, G., Melcarne, A. & Lopiano, L. (2001) Deep brain stimulation of the subthalamic nucleus in Parkinson's disease: effects of variation in stimulation parameters. *J. Neurol. Neurosurg. Psychiatr.*, **71**, 215–219.
Rubin, J.E. & Terman, D. (2004) High frequency stimulation of the subthalamic nucleus eliminates pathological thalamic rhythmicity in a computational model. *J. Comput. Neurosci.*, **16**, 211–235.
Rudolph, M. & Destexhe, A. (2006) Integrate and fire neurons with high conductance state dynamics for event driven stimulation strategies. *Neural Comput.*, **18**, 2146–2210.
Smith, Y., Bevan, M.D., Shink, E. & Bolam, J.P. (1998) Microcircuitry of the direct and indirect pathways of the basal ganglia. *Neuroscience*, **86**, 353–387.
Tai, C.H., Boraud, T., Bezard, E., Bioulac, B., Gross, C. & Benazzouz, A. (2003) Electrophysiological and metabolic evidence that high frequency stimulation of the subthalamic nucleus bridles neuronal activity in the subthalamic nucleus and the substantia nigra reticulate. *FASEB J.*, **17**, 1820–1830.
Terman, D., Rubin, J.E., Yew, A.C. & Wilson, C.J. (2002) Activity patterns in a model for the subthalamopallidal network of the basal ganglia. *J. Neurosci.*, **22**, 2963–2976.
Trottenberg, T., Kupsch, A., Schneider, G.H., Brown, P. & Kuhn, A.A. (2007) Frequency dependent distribution of local field potential activity within the subthalamic nucleus in Parkinson's disease. *Exp. Neurol.*, **205**, 287–291.
Wichmann, T., Kliem, M.A. & Soares, J. (2002) Slow oscillatory discharge in the primate basal ganglia. *J. Neurophysiol.*, **87**, 1145–1147.
Williams, S.R. & Stuart, G.J. (2000) Action potential backpropagations and the somato-dendritic distribution of ion channels in thalamocortical neurons. *J. Neurosci.*, **20**, 1307–1317.
Wilson, C.L., Cash, D., Galley, K., Chapman, H., Lacey, M.G. & Stanford, I.M. (2006) Subthalamic nucleus neurones in slices from MPTP-lesioned mice show irregular, dopamine-reversible firing pattern changes, but without synchronous activity. *Neuroscience*, **143**, 565–572.
Zhou, Q., Godwin, D.W., O'Malley, D.M. & Adams, P.R. (1997) Visualization of calcium influx through channels that shape the burst and tonic firing modes of thalamic relay cells. *J. Neurophysiol.*, **77**, 2816–2825.

Appendix

Thalamocortical relay neuron model

Both multi-compartment and single-compartment TC relay neuron models included traditional fast spike-generating currents I_{Na} and I_K, and a low threshold calcium current I_T, which plays a vital role in the generation of action potentials after hyperpolarizing input. In addition, a hyperpolarization-activated cation current I_h, a slowly activating potassium current I_{Ks}, and sodium and potassium leak currents I_{Naleak} and I_{Kleak}, which determine the resting membrane potential of the TC relay neuron were included. I_T used the Goldman–Hodgkin–Katz current equation while all other currents I_{Naleak}, I_{Kleak}, I_{Na}, I_K, I_h and I_{Ks} used the Nernst equation to incorporate the ionic driving force. Ionic concentrations were assumed to be constant under the conditions present in our study. Voltage-dependent currents were modelled using the Hodgkin–Huxley formalism and reflect well-established parameters for the TC relay neuron (Huguenard & McCormick, 1992; McCormick & Huguenard, 1992; Destexhe *et al.*, 1998; McIntyre *et al.*, 2004).

Ion currents described using the standard Hodgkin–Huxley model can be represented using the following general form:

$$I_{ion} = g_{ion} m^a h^b (V_m - E_{ion})$$

where g_{ion} is the maximum ion channel conductance, m is the activation gating variable, h is the inactivation gating variable and E_{ion} is the reversal potential. Time and voltage dependency of a gating variable (w) can be described by a time constant (τ_w) and a steady-state (w_∞)value.

$$\tau_w = \frac{1}{\alpha_w + \beta_w}$$

$$w_\infty = \frac{\alpha_w}{\alpha_w + \beta_w}$$

$$\frac{dw}{dt} = \frac{w_\infty - w}{\tau_w}.$$

Membrane dynamics and ion current descriptions are based on the modelling and experimental work of Destexhe *et al.* (1998), McCormick & Huguenard (1992), Huguenard & McCormick (1992) and McIntyre *et al.* (2004). In the model, time is in ms, voltages are in mV and ion concentrations are in mM. In the reduced single-compartment model, currents are in $\mu A/cm^2$

and maximum ion channel conductance is in mS/cm^2. The single-compartment model is implemented in MATLAB. In the multi-compartment model, currents are in mA/cm^2 and maximum ion channel conductance is in S/cm^2. The multi-compartment model is implemented in NEURON. Equations describing ion channel activation and inactivation gating variables are temperature corrected for 36°C.

Soma and dendrite sodium current

$$I_{N_a} = g_{Na} m^3 h (V_m - E_{Na})$$

$$\alpha_m = \frac{0.32(-(V_m + 55))}{[e^{(-(V_m+55))/4} - 1]}$$

$$\beta_m = \frac{0.28(V_m + 28)}{[e^{(V_m+28)/5} - 1]}$$

$$\alpha_h = 0.128 e^{-\frac{(V_m+51)}{18}}$$

$$\beta_h = \frac{4}{[e^{-(V_m+28)/5} + 1]}.$$

Soma and dendrite potassium current

$$I_K = g_K m^4 (V_m - E_K)$$

$$\alpha_m = \frac{0.032(-(V_m + 63.8))}{[e^{(-(V_m+63.8))/5} - 1]}$$

$$\beta_m = 0.5 e^{-\frac{(V_m+68.8)}{40}}.$$

Soma and dendrite hyperpolarization-activated cation current

$$I_h = g_h m^3 (V_m - 43)$$

$$\tau_m = \frac{1}{e^{(-15.45-(0.086 V_m))}} + e^{(-1.17+0.0701 V_m)}$$

$$m_\infty = \frac{1}{e^{(V_m+85)/5.5} + 1}.$$

Soma and dendrite slowly activating potassium current

$$I_{Ks} = g_{Ks} m (0.4h1 + 0.6h2)(V_m - E_K)$$

$$\tau_m = 2.5 + \frac{0.253}{e^{\left(\frac{V_m-81}{25.6}\right)} + e^{\left(-\frac{(V_m+132)}{18}\right)}}$$

$$m_\infty = \left(\frac{1}{1 + e^{\left(-\frac{V_m+43}{17}\right)}}\right)^4$$

$$\tau_{h1} = 30.4 + \frac{0.253}{e^{\left(\frac{V_m-1329}{200}\right)} + e^{\left(-\frac{(V_m+130)}{7.1}\right)}}$$

$$h1_\infty = \left(\frac{1}{1 + e^{\left(\frac{V_m+58}{10.6}\right)}}\right).$$

$$\text{If } V_m \leq -70\ \tau_{h2} = \tau_{h1}; \quad \text{else } \tau_{h2} = 2260$$

$$h2_\infty = h1_\infty.$$

The T-type calcium current is described by the Goldman–Hodgkin–Katz ion current equation.

Soma and dendrite T-type calcium current

$$I_T = P_{CaT} m^2 h G(V_m, Ca_i, Ca_o)$$

$$G(V_m, Ca_i, Ca_o) = \left(\frac{z^2 F^2 V_m}{RT}\right)\left(\frac{Ca_i - Ca_o e^{-\frac{zFV_m}{RT}}}{1 - e^{-\frac{zFV_m}{RT}}}\right)$$

$$\frac{dCa_i}{dt} = \left(\frac{0.00024 - Ca_i}{5}\right) - \frac{I_T k}{zFd}$$

$$\tau_m = 0.204 + \frac{0.333}{e^{\left(-\frac{V_m+135}{16.7}\right)} + e^{\left(\frac{V_m+19.8}{18.2}\right)}}$$

$$m_\infty = \frac{1}{1 + e^{\left(-\frac{V_m+60}{6.2}\right)}}.$$

$$\text{If } V_m < -80 \tau_h = 0.333 e^{\left(\frac{V_m+470}{66.6}\right)}; \quad else \tau_h = 9.33 + 0.333 e^{-\left(\frac{V_m+25}{10.5}\right)}$$

$$h_\infty = \frac{1}{1 + e^{\left(\frac{V_m+84}{4}\right)}}.$$

P_{CaT} is the maximum T-type calcium channel permeability in cm/s and Ca_o is 2 mM. z is the charge of a calcium ion, F is the Faraday's constant in J/(V mol), R is the gas constant in J/(K mol) and T is the absolute temperature in Kelvin. k is a unit conversion factor and is equivalent to 10 when d is 1 μm and I_T is in μA/cm^2. In the multi-compartment model, P_{CaT} is set at 0.0001 cm/s at the soma, 0.0004 cm/s at the proximal dendrites (defined as dendrites 0–45 μm away from the soma) and 0.00005 cm/s at the medial (45–90 μm away from the soma) and distal dendrites (>90 μm away from the soma) (Zhou *et al.*, 1997; Williams & Stuart, 2000; Destexhe & Sejnowski, 2003; McIntyre *et al.*, 2004; Rhodes & Llinas, 2005). In the single-compartment model, maximum T-type Ca^{2+} permeability is set at 0.0001 cm/s (Huguenard & McCormick, 1992; McCormick & Huguenard, 1992).

Network model

The membrane potential of the single-compartment STN neuron is represented by:

$$C_m \frac{dV_{STN}}{dt} = -(I_L + I_{Na} + I_K + I_T + I_{Ca} + I_{AHP} + I_{GPe-STN} + I_{CTX-STN} + I_{DBS}).$$

The membrane potential of the single-compartment GPe neuron is represented by:

$$C_m \frac{dV_{GPe}}{dt} = -(I_L + I_{Na} + I_K + I_T + I_{Ca} + I_{AHP} + I_{GPe-GPe} + I_{STN-GPe} + I_{Striatum-GPe}).$$

The membrane potential of the single-compartment GPi neuron is represented by:

$$C_m \frac{dV_{GPi}}{dt} = -(I_L + I_{Na} + I_K + I_T + I_{Ca} + I_{AHP} + I_{GPe-GPi} + I_{STN-GPi} + I_{Striatum-GPi}).$$

I_L is the leak current, I_{Na} is the fast sodium current, I_K is the fast potassium current, I_T is the low-threshold Ca^{2+} current, I_{Ca} is the high-threshold Ca^{2+} current and I_{AHP} is the Ca^{2+}-activated potassium current. Refer to Rubin & Terman (2004) and Terman *et al.* (2002) for parameter values and equations describing the ionic currents.

Synaptic input model

Synaptic currents $I_{GPe\text{-}GPe}$, $I_{GPe\text{-}GPi}$, $I_{GPe\text{-}STN}$, $I_{STN\text{-}GPi}$ and $I_{STN\text{-}GPe}$ are modelled as:

$$I_{\alpha-\beta} = g_{\alpha-\beta}(V_\beta - E_{\alpha-\beta}) \sum_j {s^j}_\alpha$$

$$\frac{ds_\alpha^j}{dt} = A_\alpha (1 - s_\alpha^j) H(V_\alpha - \theta_\alpha) - B_\alpha s_\alpha$$

α represents the pre-synaptic nucleus and β represents the post-synaptic nucleus. For $I_{GPe\text{-}GPe}$, $I_{GPe\text{-}GPi}$, $I_{GPe\text{-}STN}$, $I_{STN\text{-}GPi}$ and $I_{STN\text{-}GPe}$, $g_{\alpha-\beta}$ and $E_{\alpha-\beta}$ are equivalent to (0.3, −85), (0.75, −100), (0.3, −100), (0.3, 0), (0.3, 0).

For all synaptic currents (i.e. $I_{GPe\text{-}GPe}$, $I_{GPe\text{-}GPi}$, $I_{GPe\text{-}STN}$, $I_{STN\text{-}GPi}$ and $I_{STN\text{-}GPe}$) A_α, B_α and θ_α are equivalent to 5, 0.25 and −10 mV, respectively. Projection from striatum to GPe ($I_{Striatum\text{-}GPe}$) is represented as a constant inhibitory current and the value is set at −5 pA/μm^2.